Anhydrous Melting and Crystallization of Granite from the Transition Zone of the Qilian Orogenic Belt, NW China: An Experimental Study at Atmospheric Pressure

Chiao-wen Liaw[1], Teh-Ching Liu[1,*], Yoshiyuki Iizuka[2], Houng-Yi Yang[3]

ABSTRACT

Granite from the transition zone of the Huang Yang Dam in the Qilian orogenic belt, NW China, is studied using a high-temperature furnace at atmospheric condition. Twenty-two runs are made to locate the liquidus temperature, the solidus temperature, and the melting interval of the granite of Huang Yang Dam, Gansu Province. The experimental temperatures range from 1010°C to 1297°C. The duration time is between thirty hours to sixteen days and two hours. Compositions of glass and phenocrysts are analyzed with an electron microprobe.

The experimental results show that the liquidus temperature of the granitic melt is measured at 1296°C and the solidus temperature is lower than 1010°C. The melting interval is higher than 286°C. The liquidus mineral is zircon. The following phases are silica phase (1278°C), hematite (1269°C), titanomagnetite (1257°C), and plagioclase (1186°C). Sphene and apatite are estimated to appear at approximately 1092°C. Finally, the K-feldspar appears at 1057°C. As temperature decreases, the residual melts become depleted in iron, aluminum, calcium, and magnesium; but enriched in silicon and potassium. The differentiated melts of the granitic melt became plagioclase-depleted and quartz-enriched through fractional crystallization.

(Key words: Granite, Qilian fold belt, Experiment, Melt)

[1] Department of Earth Sciences, National Taiwan Normal University, Taipei, Taiwan, ROC

[2] Institute of Earth Sciences, Academia Sinica, Taipei, Taiwan, ROC

[3] Department of Earth Sciences, National Cheng Kung University, Tainan, Taiwan, ROC

* *Corresponding author address:* Prof. Teh-Ching Liu, Department of Earth Sciences, National Taiwan Normal University, Taipei, Taiwan, ROC; E-mail: liutc@ntnu.edu.tw

1. INTRODUCTION

The Qilian fold belt is located in the northwestern part of China (Fig. 1). It covers parts of the Qinghai and Gansu provinces. The Qilian orogenic fold belt consists of the Corridor transitional zone, North Qilian fold belt, Central Qilian uplift, and South Qilian fold belt (Feng and Wu 1992). It extends in the NWW-SEE direction with an approximate length of 1200 km and a width of roughly 250 to 300 km.

There are many tectonic models proposed to interpret the evolutions of the Qilian fold belt (e.g., Wang and Liu 1981; Xu et al. 1994; Zuo and Wu 1997). Jeng (1999) suggested that the granite at Huang Yang Dam was formed as a remnant arc in the back arc basin. There are two main models for the origin of granites: the fractional crystallization model, and the anatexis model. Bowen (1928, 1937, 1948) and Tuttle and Bowen (1958) proposed that granite could be produced by fractional crystallization of basaltic magma. Schairer and Yoder (1960), Winkler et al. (1975), and Winkler and Breitbart (1978) demonstrated that fractional crystallization of basaltic magmas could produce residual melts enriched in quartz and feldspar. Anatexis, the
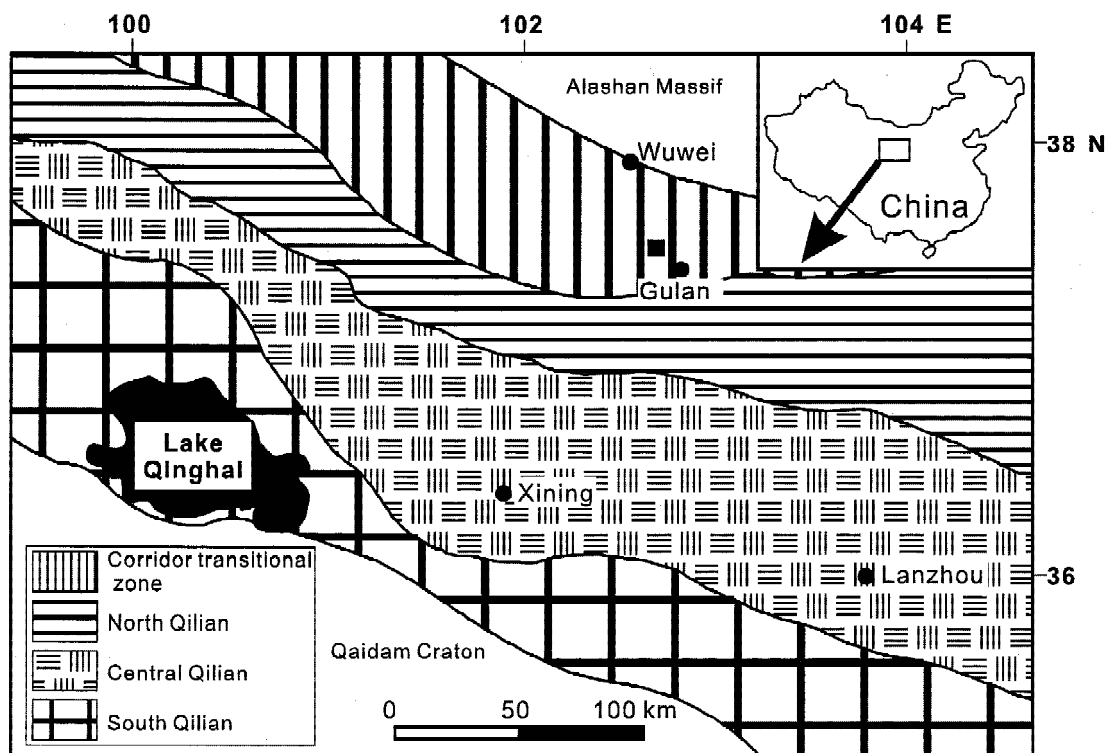

Fig. 1. Simplified tectonic map and principal units of the Qilian Fold Belt (modified from Zuo et al. 1996). Symbol: solid square: sample locality.

partial melting of preexisting rocks, is another way of producing granitic melts (Green and Ringwood 1968; Holloway and Burnham 1972; Helz 1976; Spulber and Rutherford 1983; Beard and Lofgren 1991). Of the granites all over the world, more than one hundred were compiled on the initial $^{87}Sr/^{86}Sr$ ratios by Faure and Powell (1972). Granites with low initial $^{87}Sr/^{86}Sr$ ratios are quite compatible with both the anatexis of a basaltic rock, and the fractional crystallization hypotheses. The granites with high initial $^{87}Sr/^{86}Sr$ ratios, however, are most likely to be formed by crustal anatexis.

In this study, Qilian granite was tested to estimate the solidus temperature, liquidus temperature, and melting interval of the granitic melt. The synthesized phases were analyzed with an electron microprobe, and were compared with the minerals of the granite in nature. The purpose of this study was to estimate the temperature range for the formation of the granite.

2. EXPERIMENTAL METHOD

2.1 Starting Material

The granite sample collected at Huang Yang Dam is holocrystalline, and is composed of K-feldspar, plagioclase, sub-transparent quartz, and biotite. The minerals are coarse-grained (up to 2 cm) and inequigranular. The accessory minerals include apatite, sphene, garnet, and zircon. Opaque minerals are mainly magnetite and ilmenite. About 2.5 kg of the natural granite were collected and crushed into chips. All the chips were ground into powder and passed through a 200-mesh sieve. The fine powder was kept in a desiccator as starting material for the experiments. The analysis for major elements of the powdered sample was carried out by an X-ray fluorescence (XRF) spectrometry on $Li_2B_4O_7$ fused glassy disks at the Institute of Geology of the National Taiwan University.

2.2 Apparatus and Procedures

The analytical settings, standards and mass absorption corrections for the XRF analysis of the Qilian granite were the same as described by Lee et al. (1997). The melting experimental techniques at atmospheric pressure were largely similar to those reported by Liu et al. (1997). About 0.8g of rock powders were contained in platinum envelopes, suspended in a one atmosphere vertical-quenched furnace and quenched in the water at the end of each run. No water was added to the system. The volatiles in the rock powders were expelled at a high temperature. All temperatures were measured using a $Pt - Pt_{87}Rh_{13}$ thermocouple with a precision of +/- 1°C. Based on the calibrations with the liquidus temperature of synthetic diopside ($CaMgSi_2O_6$) (Liu et al. 1997), all temperatures were corrected to be on the International Practical Temperature Scale of 1968 (Biggar 1972). Durations of experiments ranged from thirty hours to sixteen days and two hours.

2.3 Identification and Analysis of Phases

Experimental charges were mounted in epoxy and polished in longitudinal section. Phases

in the run products were first identified microscopically in reflected light. Characteristic relief, reflectivity, and crystal habit were used for phase identification, along with electron micro-probe analysis and back-scattered electron imaging in questionable cases. Mineral identification and quantitative chemical analyses were made with a JEOL EPMA JXA-8900R at the Institute of Earth Sciences, Academia Sinica in Taipei. The operated beam condition utilized was 15 kV, 10 nA, and 2 μm defocused beam for the acceleration voltage, beam current and beam size, respectively. Analysis points were carefully selected within the secondary and the back-scattered electron images. The quantitative data were corrected as oxides with standard calibration by the Phi-rho-z (PR-ZAF) method, which is a matrix correction with factors of atomic number (Z), absorption (A) and fluorescence (F) and depth distribution function (ρx), which represents the X-ray intensity per unit mass depth (ρz) (Philibert & Tixier 1968; Reed 1993). Synthetic and natural chemical-known materials were used as standards: wollatonite for Si and Ca, rutile for Ti, corundum for Al, chrome-oxide for Cr, fayalite for Fe, tephroite for Mn, pyrope for Mg, albite for Na, and adularia for K. The relative standard deviations of analysis for all 10-elements are less than 1.0% (Iizuka 1996).

The duration time of analysis for each element was 20 seconds, 10 seconds on the peak and 5 seconds each on the upper and lower side of the baseline. Grains of minerals in the quenched products chosen for analysis were usually larger than 10 μm in diameter and the diameter of analyzed glass pools was usually larger than 30 μm. The Igpet99 computer program was used to calculate the CIPW norm of the granite and glasses. Igpet99 is a commercial software supplied by Terra Softa Inc., New Jersey, U. S. A.

3. RESULTS AND DISCUSSIONS

3.1 The Granite of Huang Yang Dam

The mode of the granite components was estimated to be quartz (25.8 vol.%), K-feldspar (24.7 vol.%), plagioclase (26.6 vol.%) and biotite (22.9 vol.%). Most of the quartz, K-feldspar, plagioclase, and biotite grains are larger than 0.7 mm. The K-feldspar and plagioclase of the granite were analyzed with an electron microprobe. The compositions are listed in Table 1. The anorthite (An) content in plagioclase is about 27% with little variations in fourteen analyses. Minor zoning was observed in plagioclase, and it is classified as granite based on IUGS classification (Streckeisen 1976). Under the microscope, euhedral to subhedral zircon usually appear as inclusions in sphene, magnetite, ilmenite, or quartz. Magnetite and ilmenite are included in quartz, plagioclase, K-feldspar or biotite. Apatite is euhedral, and is also included in quartz, magnetite, plagioclase, or K-feldspar. Sphene is usually euhedral and embedded in plagioclase and biotite. Garnet is included in plagioclase and K-feldspar. Small plagioclase is a component of K-feldspar and biotite. Small quartz is also included in biotite. The textural relationships among the minerals imply that zircon, magnetites, ilmenite, apatite, and sphene appear earlier than plagioclase, K-feldspar, and biotite. The whole-rock was analyzed by XRF and the compositions are listed in Table 2. The alumina-saturation index (A/CNK) is 1.10, which is peraluminous. The granite is of the I-type.

Table 1. Chemical compositions of the K-feldspar and plagioclase of the granite in this study.

Mineral	K-feldspar	Plagioclase
Avg. of	9	14
Wt.%		
SiO_2	63.68 (0.20)[1]	60.89 (0.87)
TiO_2	0.04 (0.04)	0.01 (0.02)
Al_2O_3	18.63 (0.15)	24.27 (0.57)
MgO	0.00 (0.00)	0.01 (0.01)
FeO	0.03 (0.03)	0.06 (0.04)
CaO	0.01 (0.01)	5.58 (0.65)
Na_2O	1.21 (0.19)	8.30 (0.38)
K_2O	15.05 (0.45)	0.15 (0.06)
Cr_2O_3	0.04 (0.05)	0.02 (0.03)
MnO	0.00 (0.00)	0.02 (0.02)
Total	98.68	99.32
O=8		
Si	2.975	2.722
Ti	0.001	0.000
Al	1.026	1.279
Mg	0.000	0.001
Fe	0.001	0.002
Ca	0.000	0.268
Na	0.110	0.719
K	0.897	0.009
Cr	0.001	0.001
Mn	0.000	0.001
Total	5.013	5.001
An[2]	0	27
Ab[3]	11	72
Or[4]	89	1
Total	100	100

[1] Standard deviations of the mean; [2] An = $CaAl_2Si_2O_8$; [3] Ab = $NaAlSi_3O_8$; [4] Or = $KAlSi_3O_8$.

Table 2. Whole rock composition of the granite in this study.

XRF analysis	Wt.%	CIPW norm	%
SiO_2	67.49		
TiO_2	0.85	Qz	29.84
Al_2O_3	14.87	Or	20.98
Fe_2O_3	5.07	Ab	24.79
MgO	1.36	An	11.56
CaO	2.66	C	1.97
Na_2O	2.93	Hy	3.39
K_2O	3.55	Ilm	0.17
P_2O_5	0.25	Hem	5.07
MnO	0.08	Ap	0.58
L. O. I.	1.15	Ru	0.76
Total	100.26	Total	99.11

3.2 Experimental Runs at Atmospheric Pressure

Twenty-two runs were performed over a range of temperatures from 1010 to 1297°C at atmospheric pressure to locate the liquidus temperature, the solidus temperature, and the melting interval of the granitic melt (Table 3). The liquidus temperature of the granitic melt was determined to be 1296°C. Zircon is the first phase to crystallize at near-liquidus. Lowering the temperature causes successive crystallization of silica phase, hematite (magnetite at temperatures lower than about 1128°C), titanomagnetite (ilmenite at 1034°C and 1010°C), and then plagioclase. The crystallization sequence of the granitic melt at atmospheric pressure is as follows: zircon (1296°C), silica phase (1278°C), hematite (1269°C), titanomagnetite (1257°C), plagioclase (1186°C). Sphene and apatite were estimated to appear at about 1092°C. Finally, the K-feldspar appeared at 1057°C. Biotite was not successively synthesized because the experiments were performed at atmospheric pressure under anhydrous condition. The mode of biotite in Huang Yang granite is 22.9%. The hydrous experiments were performed at a high pressure to provide more constraints to evaluate the physical condition for the formation of Huang Yang granite. At atmospheric pressure, anhydrous synthetic granites start to melt at

Table 3. Melting experiments at atmospheric pressure.

Run no.	Temp. (℃)	Time (dd:hh:mm)	Phase(s)[1]
A12	1297	06:00:00	Gl
A11	1295	03:00:00	Gl + Zr
A10	1287	02:08:00	Gl + Zr
A24	1281	03:02:55	Gl + Zr
A09	1275	01:06:00	Gl + Zr + Sl
A22	1274	03:12:00	Gl + Zr + Sl
A25	1263	03:23:00	Gl + Zr + Sl + Hm
A23	1251	03:09:15	Gl + Zr + Sl + Hm + Tm
A15	1228	04:01:30	Gl + Zr + Sl + Hm + Tm
A17	1209	07:09:10	Gl + Zr + Sl + Hm + Tm
A16	1204	04:20:15	Gl + Zr + Sl + Hm
A28	1188	08:07:00	Gl + Zr + Sl + Hm + Tm
A30	1184	07:14:20	Gl + Zr + Sl + Hm + Tm + Pl
A26	1175	07:00:07	Gl + Zr + Sl + Hm + Tm + Pl
A18	1153	13:10:10	Gl + Zr + Sl + Hm + Pl
A20	1103	10:00:00	Gl + Zr + Sl + Mag + Pl
A32	1081	13:00:00	Gl + Zr + Sl + Mag + Tm + Pl + Sp + Ap
A27	1062	15:02:45	Gl + Zr + Sl + Mag + Tm + Pl + Sp + Ap
A33	1052	15:11:00	Gl + Zr + Sl + Mag + Tm + Pl + Sp + Ap + Kf
A31	1049	16:02:00	Gl + Zr + Sl + Mag + Tm + Pl + Sp + Ap + Kf
A29	1034	15:03:45	Gl + Zr + Sl + Mag + Ilm + Pl + Sp + Ap + Kf
A21	1010	15:09:00	Gl + Zr + Sl + Mag + Ilm + Pl + Sp + Ap + Kf

[1] Ap: Apatite; Gl: Glass; Hm: Hematite; Ilm: Ilmenite; Kf: K-feldspar; Mag: Magnetite; Ox: Fe oxides; Pl: Plagioclase; Sl: Silica; Sp: Sphene; Tm: Titanomagnetite; Zr: Zircon.

about 960°C (Tuttle and Bowen 1958). The solidus temperature of the Huang Yang Dam is estimated to be lower than 1010°C.

It is interesting and difficult to construct the paragenesis of the minerals from petrography (Hibbard 1995). Observation of the textural relationships of the minerals in thin section is limited to two dimensions. Intersection of any possible interfaces among mineral grains can yield misleading relationships under the thin sections. With this in mind, one must evaluate

the petrogenesis of the minerals in the Qilian granite tentatively with the data available. In the petrography of the granite, zircon grains are all included in sphene, magnetite, ilmenite, or quartz. It is consistent with the experimental results, which show that zircon is the nearest liquidus mineral. Magnetite and ilmentie were found as inclusions in the plagioclase and K-feldspar of the granite under the microscope. Besides, plagioclase occurred as inclusions in K-feldspar in the granite. It is consistent with the experimental results.

There are some inconsistencies between the petrography and the experimental runs. Magnetite and ilmenite appeared as inclusions in quartz under the microscope, however, quartz appears before hematite and titanomagnetite. Apatite is included in quartz, magnetite, and plagioclase in the granite. On the contrary, apatite crystallizes in the late stage in the experiments. Also, sphene is surrounded by plagioclase in thin section. Sphene crystallized after plagioclase in the experiment. We need more information about the crystallography and kinetics of the minerals to solve these complex processes.

3.3 Compositions of the Synthetic Phases

Plagioclase crystallized at 1186°C. The plagioclases synthesized at higher temperatures are rods or strings in shape. The plagioclases synthesized at lower temperatures, however, are massive and coarse (up to 60 μm). The synthesized plagioclases are homogeneous in composition and without zoning. The synthesized plagioclases were analyzed and are listed in Table 4. The An contents of synthesized plagioclases range from 27 mol% to 76 mol%. With decreasing temperature, the An contents of the synthesized plagioclases decreased and the Ab contents simultaneously increased (Fig. 2). It has been proposed that the plagioclase with An_{27} in the granite of Huang Yang Dam can be synthesized at temperature lower than 1010°C (Fig. 2) at atmospheric pressure.

The K-feldspar crystallized at 1057°C The synthesized K-feldspars were analyzed and are listed in Table 5 for comparison. With decreasing temperature, the Or contents of synthesized K-feldspars increased up to 66 mol% at 1010°C (Fig. 3). The K-feldspar of the granite with Or content of 89 mol% is expected to be synthesized at lower temperature. The iron oxides and iron-titanium oxides were also analyzed with electron microprobe, and will be provided on request.

3.4 Evolution of the Melt

The residual melts were quenched into glass. The composition of the glass in the nineteen runs, between 1297°C and 1049°C, are listed in Table 6, and are plotted versus temperature in Fig. 4. The fractionation trends (reading from high temperature, right, to low temperature, left) show enrichment in silica and potassium oxide in the later stage. The residual melts become depleted in TiO_2, Al_2O_3, MgO, total FeO, CaO and Na_2O as temperature decreases. The differentiation trend is similar to that found by Izbekov et al. (2004).

The nineteen glass compositions are also plotted in Harker's variation diagrams (Fig. 5). The variations of the silica contents make Harker's diagrams complicated. Without the experimental data at a specific temperature, we can only assume that the differentiation trend went

Table 4. Chemical compositions of the synthesized plagioclases in this study.

Run no.	A30	A26	A18	A20	A32	A27	A31	A29	A21
T (°C)	1184	1175	1153	1103	1081	1062	1049	1034	1010
Avg. of	5	6	3	4	6	9	5	3	5
SiO_2	54.61 (2.88)[1]	50.16 (2.97)	57.12 (1.48)	59.57 (0.76)	61.77 (1.55)	62.08 (0.98)	60.95 (1.26)	61.92 (0.20)	61.74 (1.05)
TiO_2	0.10 (0.05)	0.11 (0.04)	0.11 (0.03)	0.02 (0.02)	0.03 (0.04)	0.03 (0.02)	0.03 (0.02)	0.05 (0.04)	0.04 (0.03)
Al_2O_3	26.31 (1.78)	29.88 (1.64)	27.48 (1.12)	24.20 (0.33)	23.83 (0.60)	23.77 (0.49)	24.66 (0.79)	23.72 (0.42)	23.78 (0.81)
MgO	0.31 (0.20)	0.31 (0.12)	0.26 (0.05)	0.04 (0.00)	0.02 (0.01)	0.03 (0.04)	0.01 (0.01)	0.03 (0.00)	0.02 (0.02)
FeO	1.47 (0.24)	1.82 (0.52)	1.30 (0.07)	0.19 (0.04)	0.21 (0.06)	0.21 (0.08)	0.15 (0.03)	0.16 (0.02)	0.21 (0.05)
CaO	11.08 (1.35)	14.14 (2.02)	11.44 (0.94)	7.55 (0.46)	6.37 (0.79)	5.76 (0.52)	6.25 (0.82)	5.50 (0.07)	5.73 (0.87)
Na_2O	3.41 (0.24)	2.14 (1.05)	3.78 (0.37)	5.77 (0.24)	6.13 (0.13)	5.96 (0.16)	6.14 (0.23)	6.34 (0.21)	6.16 (0.22)
K_2O	0.94 (0.53)	0.53 (0.17)	0.87 (0.21)	1.20 (0.17)	1.89 (0.35)	2.57 (0.42)	2.44 (0.61)	2.83 (0.23)	2.66 (0.72)
Cr_2O_3	0.02 (0.03)	0.01 (0.03)	0.00 (0.00)	0.02 (0.00)	0.02 (0.02)	0.02 (0.04)	0.02 (0.04)	0.00 (0.00)	0.00 (0.00)
MnO	0.03 (0.04)	0.09 (0.07)	0.02 (0.03)	0.05 (0.05)	0.00 (0.00)	0.04 (0.05)	0.10 (0.06)	0.00 (0.00)	0.03 (0.03)
Total	98.28	99.21	102.38	98.61	100.26	100.48	100.73	100.54	100.36
O=8									
Si	2.518	2.319	2.525	2.697	2.746	2.757	2.707	2.754	2.750
Ti	0.004	0.004	0.004	0.001	0.001	0.001	0.001	0.002	0.001
Al	1.431	1.630	1.431	1.291	1.249	1.244	1.291	1.243	1.248
Mg	0.021	0.022	0.017	0.002	0.001	0.002	0.001	0.002	0.001
Fe	0.057	0.071	0.048	0.007	0.008	0.008	0.006	0.006	0.008
Ca	0.548	0.702	0.542	0.366	0.304	0.274	0.297	0.262	0.274
Na	0.305	0.191	0.324	0.507	0.529	0.513	0.529	0.546	0.532
K	0.055	0.031	0.049	0.069	0.107	0.146	0.138	0.161	0.151
Cr	0.001	0.000	0.000	0.001	0.001	0.001	0.001	0.000	0.000
Mn	0.001	0.003	0.001	0.002	0.000	0.002	0.004	0.000	0.001
Total	4.941	4.973	4.941	4.944	4.945	4.947	4.974	4.975	4.966
An^2	62	76	59	39	32	29	31	27	28
Ab^3	34	21	36	54	56	55	55	56	56
Or^4	4	3	5	7	12	16	14	17	16
Total	100	100	100	100	100	100	100	100	100

[1] Standard deviations of the mean; [2] An = $CaAl_2Si_2O_8$; [3] Ab = $NaAlSi_3O_8$; [4] Or = $KAlSi_3O_8$.
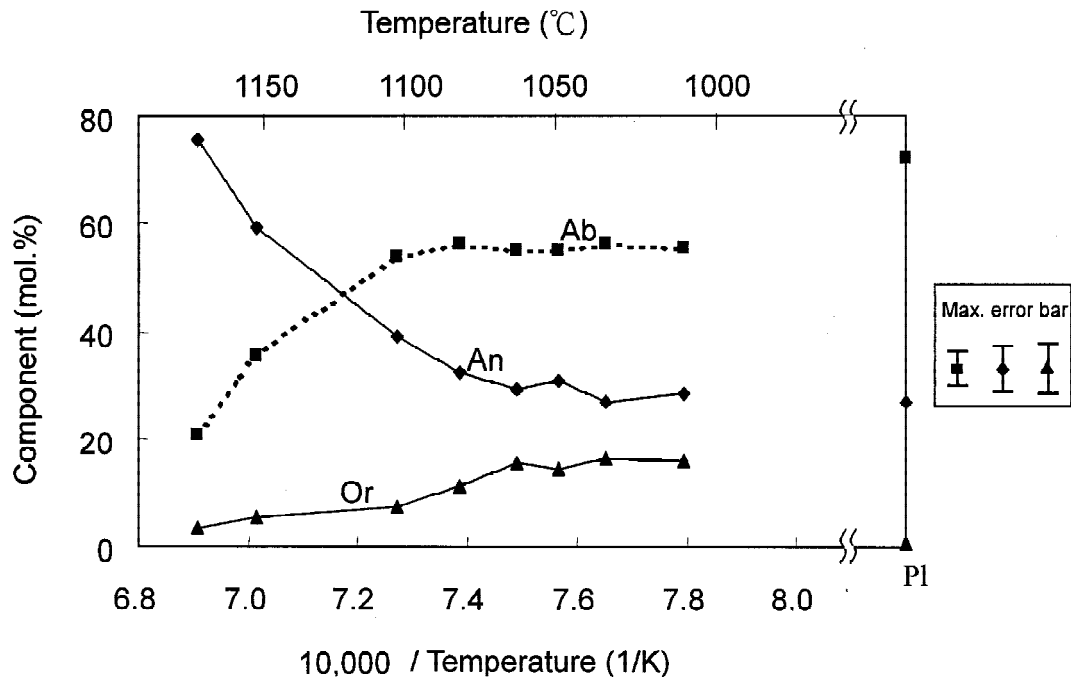
Fig. 2. The variations of synthesized plagioclase compositions versus
temperatures. The composition of natural plagioclase is also plotted in
the diagram for comparison. Ab = $NaAl_3Si_3O_8$, An = $CaAlSi_2O_8$, Or =
$KAlSi_3O_8$, Or = natural orthoclase in the granite.

from low silica content to high silica content. As the residual melts become enriched in SiO_2,
they become depleted in MgO, Al_2O_3, total FeO, CaO, and TiO_2, but enriched in K_2O. The
differentiation trend of the residual melts extend from a compositional range enriched in alkali
in the late stage, which is consistent with the results found in the felsic igneous rocks with
increasing degree of magmatic differentiation all over the world (e.g., McBirney and Aoki
1968; Bateman and Chappell 1979; Keller 1982; Jeng 1999; Faure 2001) (Fig. 6). The frac-
tionation was mainly controlled by the iron oxides and iron-titanium oxides. It is consistent
with the differentiation trends of the residual melts, which become depleted in iron and titanium.

Experimental studies demonstrated that fractional crystallization is capable of duplicating
major chemical trends in granitic rocks (e.g., Bowen 1928; Tuttle and Bowen 1958). The Qz,
Or, and Ab+An norms of the residual glasses were normalized to be 100% and are all plotted
in the granite with the IUGS classification (Streckeisen 1976). The trend of the fractional
crystallization shows that the differentiated melts become plagioclase-depleted and quartz-
enriched. It is consistent with the result found by Bateman and Chappell (1979) on the frac-

Table 5. Chemical compositions of the synthesized K-feldspar in this study.

Run no. T (°C) Avg. of	A31 1049 2	A29 1034 4	A21 1010 7
(wt.%)			
SiO_2	65.49 (0.57)[1]	65.88 (0.55)	65.86 (0.26)
TiO_2	0.02 (0.02)	0.03 (0.01)	0.01 (0.01)
Al_2O_3	18.90 (0.20)	19.09 (0.20)	18.75 (0.23)
MgO	0.04 (0.03)	0.01 (0.01)	0.00 (0.00)
FeO	0.19 (0.06)	0.14 (0.02)	0.14 (0.03)
CaO	0.76 (0.17)	0.58 (0.12)	0.41 (0.13)
Na_2O	4.12 (0.15)	3.93 (0.24)	3.54 (0.10)
K_2O	9.29 (0.60)	10.08 (0.26)	11.03 (0.33)
Cr_2O_3	0.08 (0.01)	0.05 (0.05)	0.02 (0.03)
MnO	0.11 (0.03)	0.04 (0.07)	0.03 (0.04)
Total	98.99	99.83	99.80
O=8			
Si	2.984	2.983	2.994
Ti	0.001	0.001	0.000
Al	1.015	1.019	1.005
Mg	0.003	0.001	0.000
Fe	0.007	0.005	0.005
Ca	0.037	0.028	0.020
Na	0.364	0.345	0.312
K	0.540	0.582	0.640
Cr	0.003	0.002	0.001
Mn	0.004	0.001	0.001
Total	4.958	4.967	4.978
An[2]	4	3	2
Ab[3]	39	36	32
Or[4]	57	61	66
Total	100	100	100

[1] Standard deviations of the mean; [2] An $= CaAl_2Si_2O_8$; [3] Ab $= NaAlSi_3O_8$; [4] Or $= KAlSi_3O_8$.
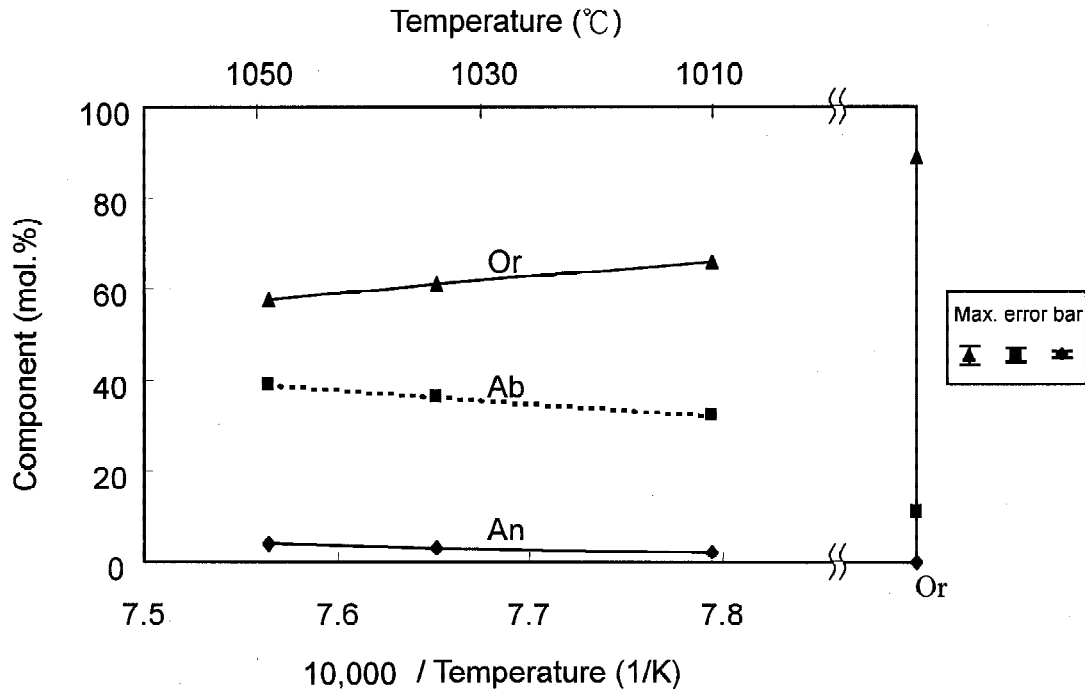
Fig. 3. The variations of synthesized orthoclase compositions versus temperatures. The composition of natural orthoclase is also plotted in the diagram for comparison. Ab = $NaAlSi_3O_8$, An = $CaAl_2Si_2O_8$, Or = $KAlSi_3O_8$, Or = natural orthoclase in the granite.

tionation trend of the Johnson Granite Porphyry in Tuolumne Intrusive Series, California, U. S. A.

4. CONCLUSIONS

The granite of Huang Yang Dam, in the Corridor transitional zone of the Qilian fold belt, consists of K-feldspar (24.7 vol.%), plagioclase (26.6 vol.%), quartz (25.8 vol.%), and biotite (22.9 vol.%). The accessory minerals include apatite, sphene, garnet, zircon, magnetite, and ilmentite. It is peraluminous.

The liquidus temperature of the granitic melt is estimated to be 1296°C. The solidus temperature of the granitic melt is lower than 1010°C. The crystallization order of the granitic melt at atmospheric pressure is constructed as follows: zircon (1296°C), quartz (1278°C), hematite (1269°C), titanomagnetite (1257°C), plagioclase (1186°C), sphene and apatite (about 1092°C), and K-feldspar (1057°C). As temperature decreases, the residual melt becomes de-

Table 6. Chemical compositions (wt.%) of the glasses in this study.

Run no.	A12	A11	A10	A24	A09	A22	A25	A23	A15	A17
T (°C)	1297	1295	1287	1281	1275	1274	1263	1251	1228	1209
Avg. of	3	10	7	3	2	3	4	3	4	3
SiO_2	69.11 (0.21)[1]	69.74 (0.83)	69.45 (0.45)	69.69 (0.48)	69.26 (0.06)	70.09 (0.50)	68.71 (0.62)	69.19 (0.14)	68.87 (0.62)	69.26 (0.83)
TiO_2	0.86 (0.01)	0.83 (0.06)	0.80 (0.06)	0.82 (0.00)	0.82 (0.08)	0.80 (0.10)	0.80 (0.04)	0.77 (0.04)	0.87 (0.07)	0.77 (0.07)
Al_2O_3	14.78 (0.06)	14.86 (0.31)	14.64 (0.20)	14.08 (0.25)	14.75 (0.34)	14.41 (0.26)	14.29 (0.39)	14.67 (0.18)	14.84 (0.22)	14.20 (0.38)
MgO	1.29 (0.02)	1.29 (0.05)	1.19 (0.04)	1.31 (0.08)	1.26 (0.02)	1.32 (0.11)	1.25 (0.06)	1.29 (0.01)	1.24 (0.01)	1.27 (0.12)
FeO	4.06 (0.18)	4.19 (0.14)	4.07 (0.14)	4.25 (0.17)	4.11 (0.01)	4.16 (0.10)	4.04 (0.37)	4.36 (0.15)	4.11 (0.09)	3.34 (0.08)
CaO	2.59 (0.04)	2.59 (0.14)	2.59 (0.10)	2.50 (0.10)	2.63 (0.04)	2.66 (0.01)	2.57 (0.12)	2.64 (0.05)	2.72 (0.13)	2.46 (0.18)
Na_2O	2.47 (0.06)	2.45 (0.15)	2.69 (0.09)	2.25 (0.09)	2.61 (0.04)	2.14 (0.05)	2.19 (0.18)	2.49 (0.14)	2.65 (0.17)	2.77 (0.09)
K_2O	3.74 (0.12)	3.84 (0.08)	3.84 (0.02)	3.51 (0.09)	3.86 (0.02)	3.37 (0.05)	3.51 (0.05)	3.54 (0.16)	3.73 (0.11)	3.80 (0.09)
Cr_2O_3	0.02 (0.02)	0.03 (0.03)	0.01 (0.01)	0.03 (0.05)	0.03 (0.02)	0.02 (0.03)	0.04 (0.03)	0.03 (0.04)	0.03 (0.03)	0.02 (0.02)
MnO	0.12 (0.06)	0.10 (0.08)	0.15 (0.04)	0.09 (0.01)	0.14 (0.05)	0.06 (0.05)	0.04 (0.03)	0.11 (0.00)	0.06 (0.04)	0.04 (0.03)
Total	99.03	99.93	99.45	98.55	99.47	99.04	97.43	99.07	99.11	97.91
CIPW Norm										
Qz	30.09	30.34	28.82	32.84	28.85	34.13	32.36	30.45	27.49	29.22
Or	22.13	22.68	22.71	20.74	22.81	19.92	20.74	20.90	22.39	22.43
Ab	20.92	20.77	22.80	19.04	22.08	18.13	18.53	21.04	23.14	23.45
An	12.83	12.84	12.84	12.40	13.05	13.20	12.75	13.10	13.63	12.19
C	1.96	1.96	1.35	2.03	1.50	2.40	2.22	1.95	1.26	1.06
Hy	9.45	9.73	9.41	9.88	9.60	9.72	9.29	10.15	9.43	8.09
Ilm	1.63	1.58	1.52	1.56	1.55	1.52	1.52	1.45	1.65	1.45
Total	99.01	99.90	99.45	98.49	99.44	99.02	97.41	99.04	98.99	97.89

[1] Standard deviations of the mean.

Table 6. Continued.

| Run no.	A16	A28	A30	A26	A18	A20	A32	A27	A31
T (°C)	1204	1188	1184	1175	1153	1103	1081	1062	1049
Avg. of	6	3	5	4	7	2	4	6	2
SiO_2	71.16 (0.76)[1]	70.02 (1.31)	69.18 (1.20)	70.27 (0.99)	73.43 (0.77)	72.88 (0.77)	72.94 (2.39)	73.57 (1.17)	72.78 (0.34)
TiO_2	0.87 (0.04)	0.64 (0.12)	0.64 (0.11)	0.60 (0.08)	0.63 (0.05)	0.47 (0.05)	0.42 (0.11)	0.38 (0.14)	0.36 (0.03)
Al_2O_3	15.01 (0.37)	14.04 (0.78)	14.53 (0.74)	14.29 (0.32)	14.20 (0.50)	13.19 (0.37)	13.01 (0.56)	12.47 (0.99)	14.04 (0.39)
MgO	1.35 (0.12)	1.23 (0.14)	1.38 (0.15)	1.29 (0.15)	1.29 (0.10)	1.16 (0.12)	0.97 (0.04)	1.05 (0.49)	0.74 (0.08)
FeO	4.00 (0.17)	2.84 (0.10)	3.02 (0.32)	2.91 (0.18)	2.58 (0.11)	1.78 (0.07)	1.84 (0.31)	1.50 (0.08)	1.27 (0.04)
CaO	2.52 (0.27)	2.61 (0.31)	2.66 (0.32)	2.55 (0.17)	2.19 (0.17)	1.32 (0.08)	1.04 (0.11)	0.80 (0.15)	0.78 (0.11)
Na_2O	2.18 (0.20)	2.37 (0.26)	2.84 (0.17)	2.38 (0.26)	2.25 (0.13)	2.44 (0.02)	2.49 (0.14)	2.31 (0.21)	1.86 (0.57)
K_2O	3.26 (0.20)	3.48 (0.08)	3.69 (0.11)	3.68 (0.06)	3.43 (0.17)	4.46 (0.11)	4.39 (0.51)	4.78 (0.47)	5.18 (0.66)
Cr_2O_3	0.03 (0.03)	0.02 (0.02)	0.01 (0.02)	0.07 (0.06)	0.00 (0.00)	0.07 (0.07)	0.00 (0.00)	0.01 (0.03)	0.15 (0.01)
MnO	0.07 (0.05)	0.10 (0.05)	0.09 (0.12)	0.09 (0.10)	0.12 (0.06)	0.14 (0.11)	0.02 (0.03)	0.10 (0.06)	0.11 (0.07)
Total	100.45	97.35	98.05	98.12	100.11	97.91	97.10	96.96	97.25
CIPW Norm									
Qz	35.82	33.51	28.66	32.90	38.83	35.80	36.74	37.51	38.48
Or	19.26	20.59	21.81	21.75	20.25	26.35	25.94	28.25	30.61
Ab	18.48	20.05	24.03	20.14	19.03	20.67	21.07	19.55	15.74
An	12.49	12.92	13.20	12.65	10.86	6.55	5.16	3.97	3.87
C	3.31	1.63	1.03	1.76	2.81	1.95	2.27	2.04	3.96
Hy	9.40	7.41	8.09	7.73	7.14	5.64	5.14	4.93	3.79
Ilm	1.65	1.22	1.22	1.14	1.19	0.89	0.80	0.72	0.68
Total	100.41	97.33	98.04	98.07	100.11	97.85	97.12	96.97	97.12
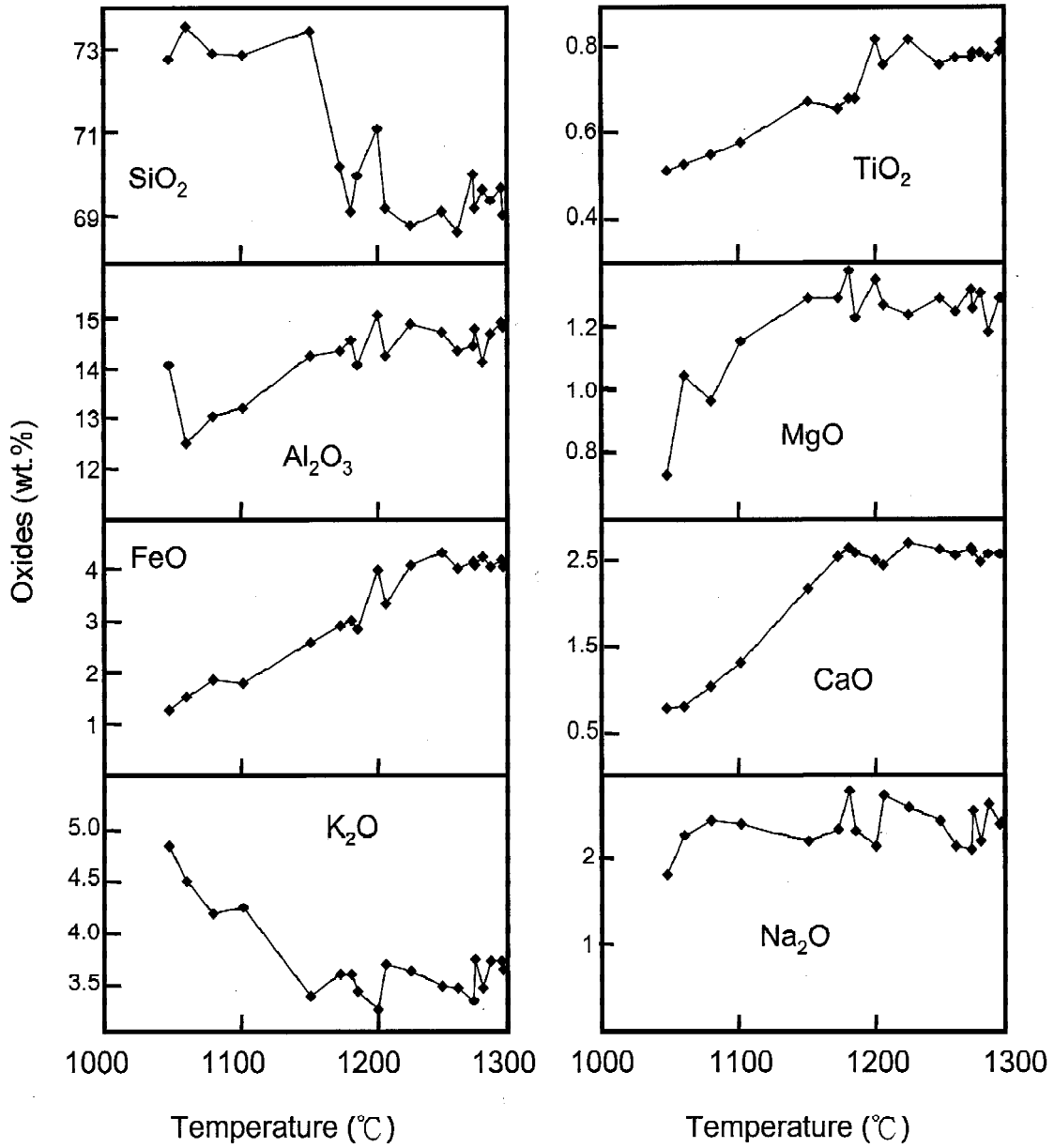
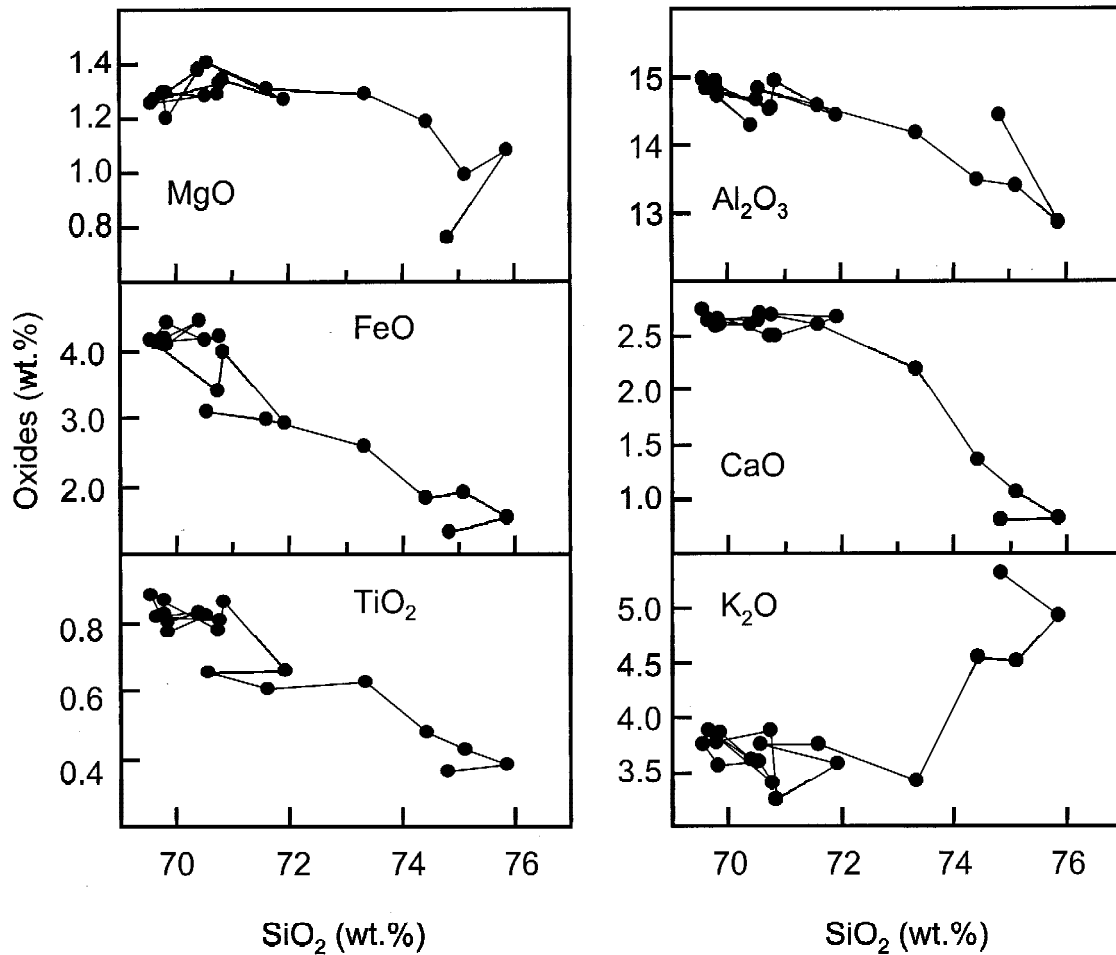*Fig. 4.* The variations of glass compositions versus temperatures.

Fig. 5. The variations of glass compositions in Harker's diagrams.

pleted in iron, aluminum, calcium, and magnesium; but enriched in silicon and potassium. The differentiated melts of the granitic magma become plagioclase-depleted and quartz-enriched through fractional crystallization.
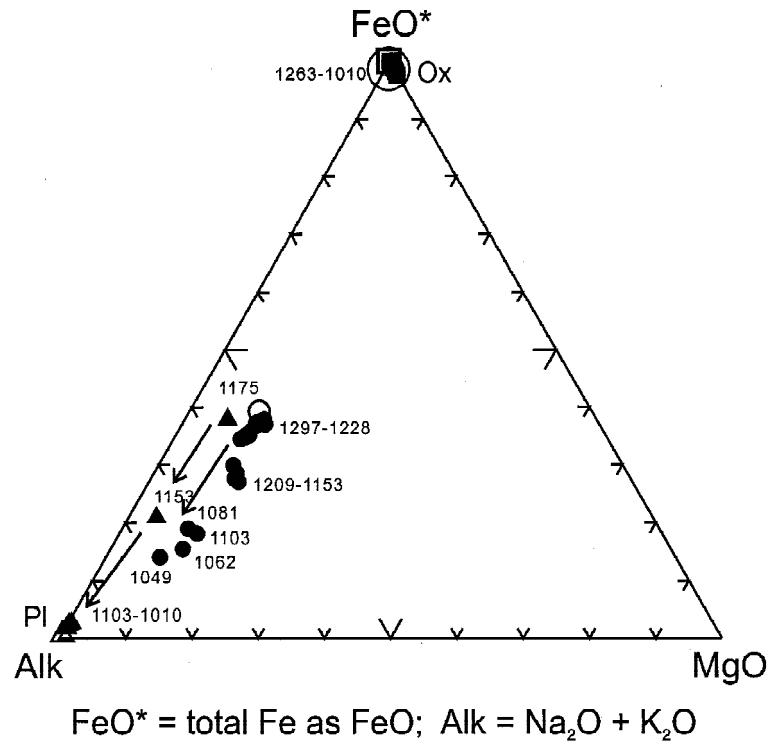
Fig. 6. The variations of glass compositions in AFM diagram. Open circle: whole rock composition of the granite; solid circles: glass composition at each temperature; open square: the oxides of the granite; solid squares: the synthesized oxides in this study; open triangle: the plagioclase of the granite; solid triangles: the synthesized plagioclase in this study; numbers: temperatures (°C).

REFERENCES

Albee, A. L., and L. Ray, 1970: Corrections factors for electron microprobe analysis of silicates, oxides, carbonates, phosphates and sulfates. *Anal. Chem.*, **42**, 1408-1414.

Bateman, P. C., and B. W. Chappell, 1979: Crystallization, fractionation, and solidification of the Tuolumne intrusive series, Yosemite National Park, California. *Geol. Soc. Am. Bull.*, **90**, 465-482.

Beard, J. S., and G. E., Lofgren, 1991: Dehydration melting and water-saturated melting of basaltic and andesitic greenstones and amphibolites at 1, 3, and 6.9 kb. *J. Petrol.*, **32**, 365-401.

Biggar, G. M., 1972: Diopside, lithium metasilicate, and the 1968 temperature scale. *Mineral. Mag.*, **38**, 768-770.

Bowen, N. L., 1928: The evolution of the igneous rocks. Princeton Univ. Press, 334 pp.

Faure, G., 2001: Origin of the igneous rocks: the isotopic evidence. Springer, Berlin, Germany, 496 pp.

Faure, G., and J. L. Powell, 1972: Strontium isotope geology, Springer-Verlag, Berlin, Heidelberg and New York, 188 pp.

Feng, Y., and H. Wu, 1992: A preliminary study on the tectonic evolution of the North Qilian and adjacent area after Paleozoic era. *Northwest Geosci.*, **13**, 61-74. (in Chinese)

Green, T. H., and A. E. Ringwood, 1968: Genesis of the calc-alkaline igneous rock suite. *Contrib. Mineral. Petrol.*, **18**, 105-62.

Helz, R. T., 1976: Phase relations of basalts in their melting range at $P_{H_2O} = 5$ kb. Part II. Melt compositions. *J. Petrol.*, **17**, 139-93.

Hibbard, M. J., 1995: Petrography to petrogenesis, Prentice Hall, New Jersey, 587 pp.

Holloway, J. R., and C. W. Burnham, 1972: Melting relations of basalt with equilibrium water pressure less than total pressure. *J. Petrol.*, **13**, 1-29.

Iizuka Y., 1996: The quantitative analysis of the rock-forming minerals by the electron micro-probe analyzer. Experimental study on the slab-mantle interaction in subduction zones and its implications for the material recycling through the subduction zones. Ph. D. Thesis. Inst. Study of the Earth's Interior, Okayama University Misasa (Japan), 88-107.

Izbekov, P., J. E. Gardner, and J. C. Eichelberger, 2004: Comelttic granophyre and dacite from Karymsky volcanic center, Kamchatka: experimental constraints for magma storage conditions. *J. Volcan. Geotherm. Res.*, **131**, 1-18.

Jeng, C. K., 1999: Petrological and Geochemical Studies of the Back-Arc Basinal Granitoids-as exemplified by the plutonic rocks from Laohushan area, east section of north Qilian Fold Belt. MS thesis, Nat. Taiwan Univ., Taipei. (in Chinese)

Keller, J., 1982. Mediterranean island arcs. In Andesites:orogenic andesites and related rocks. Thorpe, R. S. (Ed.), John Wiley & Sons, Chichester and New York, 307-325.

Lee, C. Y., J. H. Tsai, H. H. Ho, F. T. Yang, S. L. Chung, and C. H. Chen, 1997: Quantitative analysis in rock samples by an X-ray fluorescence spectrometer (I) Major elements. Abstract of 1997 An. Meet. Geol. Soc. China, 418-420. (in Chinese)

Liu, T. C., B. S. Chen, J. J. Pan, P. K. Chen, and S. Z. Wu, 1997: A preliminary report on the experimental study of the two-pyroxene andesite from Kuanyinshan, Northern Taiwan. *J. Nat. Taiwan Normal Univ.: Math., Sci., Tech.*, **42**, 53-59

McBirney, A. R., and K. Aoki, 1968: Petrology of the island of Tahiti, In: Coats, R. R., R. L. Hay, and C. A. Anderson (Eds.), Sudies in Vocanology. *Mem. Geol. Soc. Am.*, **116**, 523-556.

Philibert, J., and R. Tixier, 1968: Electron penetration and the atomic number correction in electron probe microanalysis. *Brit. J. Appl. Phys.,* **2**, 685-694.

Reed, S. J. B., 1993: Electron Microprobe Analysis, 2nd ed., Cambridge Univ. Press, Cambridge, 326 pp.

Spulber, S. D. and M. J. Rutherford, 1983: The origin of rhyolite and plagiogranite in oceanic crust: an experimental study. *J. Petrol.*, **24**, 1-25.

Streckeisen, A. L., 1976: To each plutonic rock its proper name. *Earth Sci. Rev.*, **12**, 1-33.

Tuttle, O. F., and N. L. Bowen, 1958: Origin of granite in the light of experimental studies in the system $NaAlSi_3O_8$-$KAlSi_3O_8$-SiO_2-H_2O. *Mem. Geol. Soc. Am.*, **74**, 153 pp.

Wang, Q., and X. Liu, 1981: On Caledonian polycyclic paired metamorphic belts of Qilian Mountains, northwest China. In: Huang, T. K., and C. Y. Li (Eds.), Contrib. to Tectonics of China and Adjecent Regions. Beijing: Geological Publishing House, 92-101. (in Chinese with English abstract)

Xu, Z., H. Xu, J. Zhang, H. Li, Z. Zhu, and J. Qu, 1994: The Zoulangnanshan Caledonian subductive complex in the northern Qilian Mountains and its dynamics. *Acta Geol. Sinica*, **68**, 1-14. (in Chinese with English abstract)

Zuo, G., and H. Wu, 1997: Bilateral subduction-collision mountain-building in the Early Paleozoic Mid-North Qilian, China. *Prog. Earth Sci.*, **12**, 315-323. (in Chinese with English abstract)